Applied Energy 391 (2025) 125859

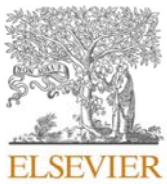

Contents lists available at ScienceDirect

Applied Energy

journal homepage: www.elsevier.com/locate/apenergy

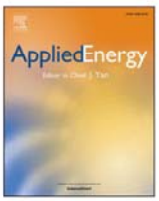

A novel double-Gaussian full wake model for wind turbines considering dependence on thrust coefficient and ambient turbulence intensity

Guo-Wei Qian [a,b,c], Takeshi Ishihara [c,*]

[a] School of Ocean Engineering and Technology, Sun Yat-sen University & Southern Marine Science and Engineering Guangdong Laboratory (Zhuhai), Zhuhai 519082, China
[b] Guangdong Provincial Key Laboratory of Information Technology for Deep Water Acoustics (Sun Yat-sen University), Zhuhai 519082, China
[c] Department of Civil Engineering, School of Engineering, The University of Tokyo, 7-3-1 Hongo, Bunkyo-ku, Tokyo 113-8656, Japan

HIGHLIGHTS

- A novel double-Gaussian full wake model is proposed to describe velocity deficits.
- The proposed model shows good agreement with LES data and measurements.
- The proposed model provides good accuracy for power prediction in the multiple wakes.

ARTICLE INFO

Keywords:
Wind turbine wakes
Wake model
Double-Gaussian
Velocity deficit
Wind farm power prediction

ABSTRACT

A novel full wake model using a double-Gaussian function is derived in this study. Firstly, the full wake characteristics under different inflow and turbine operation conditions are investigated using large eddy simulation. The ambient turbulence intensity and thrust coefficient are found to be the key parameters that determine the wake recovery rate and the distance where double-peak velocity deficits transition to one-peak distribution. A novel double-Gaussian wake model is then proposed to estimate the mean velocity deficit in both the near and far wake region. A linear wake expansion rate and non-linear Gaussian minima are demonstrated and utilized to describe the shape transition of velocity deficit from near-wake to far-wake region. All the parameters in the model are expressed as a function of thrust coefficient and ambient turbulence intensity. Finally, the proposed model is validated using a set of LES results and experimental data. The predicted velocity profiles in the near wake region by the proposed model show good agreement with LES and measurements. Furthermore, the proposed full wake model is applied to Horns Rev. offshore wind farm and provides good accuracy for power prediction in the multiple wakes as well. The applications of this new full wake model include, but are not limited to turbine layout optimization, farm control, and repower of existing wind farms.

1. Introduction

Wind energy has become one of the fastest-growing sources of renewable energy, with global installed capacity surpassing 1021 GW by 2023 [1], driven by the rapid adoption in many countries. Offshore wind farms are seeing rapid expansion due to their potential for higher capacity factors and less land-use conflict compared to onshore installations. However, as wind farms increase in scale and density, challenges such as wind turbine wakes, the regions of reduced wind speed and increased turbulence downstream of turbines, become critical to address. Wind turbine wakes cause power losses and increased fatigue loading on downstream turbines in wind farms, presenting challenges for energy production efficiency and turbine longevity. As a result, extensive research has been conducted to develop accurate models and mitigation strategies for managing wake effects [2–4]. Although high-fidelity computational fluid dynamics models can provide accurate and detailed turbulent flow field, analytical wake models are low computational cost and thus preferred to be utilized in wind farm layout design [5] and wind farm control [6], where many simulations are required to reach an optimum solution.

In the wake of a wind turbine, the velocity decreases, while the turbulence intensity increases [7]. The length of near-wake region is

* Corresponding author.
E-mail address: ishihara@bridge.t.u-tokyo.ac.jp (T. Ishihara).

https://doi.org/10.1016/j.apenergy.2025.125859
Received 13 December 2024; Received in revised form 18 March 2025; Accepted 3 April 2025

typically less than three times the diameter of the rotor [8], where the wake behavior is complicated to deal with since it is affected by the blade, nacelle and tower aerodynamics [7,9]. Wind turbines are normally located in the wind farm with a distance larger than three diameters of the rotor. Therefore, most studies have made efforts on the modelling of far wake regions, where analytical solutions of the velocity deficit can be obtained by utilizing the assumption of axisymmetric and self-similar distributions. The most widely used wake model for velocity deficit was first introduced by Jensen [10], which uses a top-hat distribution and a linearly expanding wake. The Jensen model was further developed by Frandsen [11]. Compared with the top-hat distribution, experimental data [4,12] and numerical simulations [9] have shown that the Gaussian distribution is more reasonable to explain the velocity deficit profile in the mid- to far-wake regions. Hence, it was used in most updated wake models [13–19]. However, these models lack accuracy in the near-wake region, where the Gaussian distribution is unjustified [20].

Recently, the necessity of full wake models that can not only provide good estimation in the far wake region but also accurately describe the velocity deficit in the near wake regions is raised for the following two reasons. Firstly, some onshore wind turbines tend to be closely installed with a spacing close or even below 3D [21], where the downstream turbines are significantly affected by near wake effects. Secondly, there is a need to measure the wind speed inside existing wind farms when they are repowered. Repowering involves replacing old turbines with new ones. In such cases, the wind speed measurement equipment is often forced to be installed close to the wind turbines, as permission and space constraints make it impractical to install equipment a significant distance from the turbines. Therefore, accurate wake models are required to accurately assess wind conditions. This ensures that the measurements are not influenced by the turbine wake and reflect real wind conditions. The existing full wake models are summarized in Table 1. The first type of full wake model is developed based on a super-Gaussian shape function [22], which evolves from a smooth top-hat shape in the near wake region and leads to the single-Gaussian shape in the far wake. Zhang et al. [23] also introduced the super-Gaussian function to refine the near wake model, which is then combined with four different far wake models to develop four temporal wake models aiming at capturing the time-varying nature of the wake. Wei et al. [24] applied the super-Gaussian function as well to the development of a three-dimensional wake model. However, it was found that the super-Gaussian assumption was only applicable to the high ambient turbulence cases.

Another velocity deficit distribution is based on the double-Gaussian shape function. Keane et al. [25] firstly proposed a wake model taking the double-Gaussian function to describe the velocity deficit in both near- and far-wake regions. Later, Schreiber et al. [26] found and resolved some issues in the original model of Keane et al. [25], primary concerning momentum conservation in the near-wake region. However, the streamwise function of velocity deficit still has the possibility to diverge when the thrust coefficient has a large value. Keane [27] also noted the shortcoming in the previous work and updated the model by introducing a real and complex solution of the wake deficit equations, while the complex solution does not have any physical support as the author mentioned. More recently, the wind shear effects [19], and anisotropic wake expansion [28] were also incorporated into the double-Gaussian wake model. However, in the above models, the Gaussian minima which determines the peak position of velocity deficit was assumed to be constant with a specific value. This can obtain an acceptable reproduction in the near-wake region but will lead to underestimation of velocity deficit in the far-wake region as shown in the work by Schreiber et al. [26]. Moreover, current full wake models based on double-Gaussian distribution have not carefully considered dependencies on thrust coefficient and ambient turbulence intensity. Zengler et al. [29] also noticed this problem and proposed an extension of the double-Gaussian wake model that incorporates the position of the Gaussian peaks depending on the thrust coefficient. However, it was still assumed that the peak position of velocity deficit is constant and dependencies on ambient turbulence are not included. These are key factors that significantly influence the behavior of the wake as mentioned in relevant studies [30,31]. Without considering these dependencies, wake models cannot fully capture the complex dynamics of the wake and can lead to inaccuracies in predicting the impact on downstream turbines. This highlights that a generic formulation of the double-Gaussian wake models that incorporate these factors is needed to improve the accuracy and reliability of wake models and, consequently, the optimization of wind farm layout and operation.

Section 2 describes the full wake characteristics, the derivation, and parameter identification of the novel double-Gaussian wake model. In Section 3, the proposed model is validated using numerical results of LES, experimental data of the wind tunnel tests and the field measurements, where the proposed model is compared to the conventional double-Gaussian model, super-Gaussian model and single-Gaussian model as well. The conclusions are finally summarized in Section 4.

2. Double-Gaussian wake model

Section 2.1 introduces the full wake characteristics in terms of the mean velocity field obtained from LES numerical simulations. The formulation of a novel double-Gaussian wake model is then presented,

Table 1
List of representative full wake models. $C(x)$ denotes the amplitude function of the velocity deficit and σ represents the characteristic wake width. More detailed information on model parameters can be found in the related literature.

Wake models	Shape Function of Velocity Deficit	Formulas
Blondel and Cathelain [22]	Super-Gaussian	$\Delta U/U_0 = C(x)\cdot exp\left(-\frac{r^n}{2\sigma^2}\right), C(x) = 2^{2/n-1} - \sqrt{2^{4/n-2} - \frac{nC_T}{16\Gamma(2/n)\sigma^{4/n}}}$
Wei et al. [24]	Super-Gaussian	$\Delta U/U_0 = 1 - \left(\frac{z+z_h}{z_h}\right)^{\alpha} + C(x)\cdot exp\left(-\frac{z^n}{2\sigma_z^n}\right) + \frac{\iint_{S_{e0}}(\Delta U\cdot 2a)dA}{U_0\pi r_x^2}$ $C(x) = \frac{r\left(\frac{1}{2} - \frac{1}{2}\frac{D}{d_x}\sqrt{\left(\frac{d_x}{D}\right)^2 - 2C_T}\right)}{2^{1/n}\Gamma(1/n)1/n\,\sigma} exp\left(-\frac{y^n}{2\sigma_y^n}\right)$
Schreiber et al. [26]	Double-Gaussian	$\Delta U/U_0 = C(x)\cdot\frac{1}{2}\left\{exp\left(-\frac{(r+r_{min})^2}{2\sigma^2}\right) + exp\left(-\frac{(r-r_{min})^2}{2\sigma^2}\right)\right\}$ $C(x) = \frac{M - \sqrt{M^2 - 1/2N\,C_T D^2}}{2N}, \frac{\sigma}{D} = k^*\frac{x-x_0}{D} + \varepsilon$
Keane et al. [25,27]	Double-Gaussian	$\Delta U/U_0 = C(x)\cdot\frac{1}{2}\left\{exp\left(-\frac{(r+r_{min})^2}{2\sigma^2}\right) + exp\left(-\frac{(r-r_{min})^2}{2\sigma^2}\right)\right\}$ $C(x) = \frac{M \pm \sqrt{M^2 - 1/2N\,C_T D^2}}{2N}, \frac{\sigma}{D} = k^*\frac{x^n}{D} + \varepsilon$

and the model parameter identifications are described as well in Section 2.2.

2.1. Full wake characteristics

In this study, the large eddy simulation with Smagorinsky-Lill model [32] in Fluent [33] is used to simulate wind turbine wakes. A 2.4 MW wind turbine located at the Choshi site is adopted to study the full wake characteristics. The rotor diameter is 92.0 m and the hub height is 80.0 m as shown in [20]. The influence of the rotor on the flow is modelled by using an actuator line model. The lift and drag forces are calculated using the blade element theory as shown in [34]. The numerical schemes of LES model, grid resolutions, computational domain and boundary conditions perfectly follow the setting in the reference [20]. The predicted wind turbine wake was validated by the wind tunnel test [14]. As mentioned in previous studies [35,36], the nacelle and tower may affect the coherent structures in the near wake region of a utility-scale wind turbine, while their overall impact on the mean velocity deficit and mean power output is relatively small compared to the impact caused by the blades. Therefore, to purely understand the dependency of near-wake characteristics on rotor aerodynamic forces, the nacelle and tower are not modelled in this study. Four simulations with two kinds of operating condition under the inflow with low turbulence intensity of $I_a = 3.5\,\%$ and high one of $I_a = 13.7\,\%$ are conducted. They are labelled as shown in Table 2.

The mean velocities in the wake region are displayed in Fig. 1, where the contours from LES simulations are shown in the horizontal x-y plane at the hub-height of $z = H$. It is noted that the velocity deficit distribution has double peak due to the low-speed structures in the near-wake region. A jet region (i.e. with negative velocity deficit) can be observed around the wake boundary area at low turbulence intensity cases, which is due to acceleration of the flow outside the wake region, as observed by Neunaber et al. [37]. The double-peak distribution transits to single peak in the far-wake region due to the turbulence mixing effect. For the low ambient turbulence intensity cases with I_a=3.5 %, the double-peak velocity deficits are prominent at a downwind distance of about $3D \sim 4D$, while this region is shorter with around 2D for high ambient turbulence cases with I_a=13.7 %. This implies that the level of ambient turbulence intensity has a strong impact on the transition process from double-peak deficit to single-peak deficit. Furthermore, a closer look at the wake boundary at different locations reveals that the wake width gradually widens. This is demonstrated later in Fig. 5, where the increase in σ with downstream distance indicates the wake widening, confirming that the wake expansion is occurring. It is also clear that large C_T produces stronger deficits in the near-wake region, and the locations of local minima are closer to tip side than that of small C_T cases. This is more clearly identified in Fig. 2, where the horizontal distributions at $x = 0.2D$ are plotted to illustrate the mechanism of the double-peak deficit. Black open circles and squares represent the velocity deficits ΔU normalized by the maximum deficit $\Delta U_{\max}$ for low ambient turbulence cases with I_a=3.5 % and high ambient turbulence cases with I_a=13.7 %, respectively. In addition, the distribution of blade aerodynamic force normal to the rotor dFx is also shown by red solid lines, which is normalized by the maximum value dFx_{max} as well. x denotes the streamwise direction. The thrust forces show a m-shape due to the aerodynamic characteristics of blades, where the peak value for the large C_T case locates around the mid-span range, while that for the small C_T case is closer to the blade root. The velocity deficit would present a similar distribution to that of aerodynamic force, since aerodynamic force distributions directly determine the initial velocity deficit in the near-wake region. It can be concluded that the local minimum of double peak should depend on the ambient turbulence intensity and rotor thrust coefficient as well.

Table 2
Description of four simulations.

Simulation Case	Thrust coefficient	Ambient turbulence intensity
Case 1	$C_T = 0.36$	$I_a = 3.5\,\%$
Case 2	$C_T = 0.84$	$I_a = 3.5\,\%$
Case 3	$C_T = 0.36$	$I_a = 13.7\,\%$
Case 4	$C_T = 0.84$	$I_a = 13.7\,\%$

2.2. Model formulation and parameters

Similar to the single-Gaussian wake model derivation as shown in [14,16], the axisymmetric assumption and the self-similar distribution are used for the velocity deficit in the current model. The mean streamwise velocity $U_w(x,y,z)$ in the wake region is expressed as,

$$U_w(x,y,z) = U_0(x,y,z) - \Delta U(x,r) \tag{1}$$

where $U_0(x,y,z)$ is the free stream velocity, $\Delta U(x,r)$ is the velocity deficit induced by the turbine and is assumed to be axisymmetric about the rotor axis. r denotes the radial distance from the wake center and is defined as follows:

$$r = \sqrt{y^2 + (z-H)^2} \tag{2}$$

where H is the hub height.

The non-dimensional velocity deficit is then expressed as the product of a streamwise function $F(x)$ and a radial function $\phi(r)$:

$$\Delta U(x,r)/U_h = F(x)\phi(r) \tag{3}$$

where U_h is the free stream velocity at the hub height.

According to the wake characteristics presented in Figs. 1 and 2, a double-Gaussian function is utilized for the radial function to describe the spatial distribution of the velocity deficit and is defined as,

$$\phi(r) = \frac{1}{2}\left\{\exp\left(-\frac{(r+r_{min})^2}{2\sigma^2}\right) + \exp\left(-\frac{(r-r_{min})^2}{2\sigma^2}\right)\right\} \tag{4}$$

where r_{min} is the radial position of the Gaussian extrema, σ is the standard deviation of the Gaussian function, which represents the width of each single-Gaussian profile. Fig. 3 depicts the schematic of the double-Gaussian wake model. The double-Gaussian and its constituent single-Gaussian functions are plotted by black solid lines and gray dashed lines, respectively. Blue dashed lines represent the location of the Gaussian extrema r_{min}. The half-width of velocity deficit with the Gaussian distribution $r_{1/2} = \sqrt{2ln2}\sigma$ denotes the location where the velocity deficit equals the half the maximum value, and the velocity deficit normalized by the maximum value at the twice of half-width $2r_{1/2}$ is 0.018. Accordingly, $\pm\left(r_{min} + 2\sqrt{2ln2}\,\sigma\right)$ is used to represent the double-Gaussian wake boundary, which is expressed by the orange dashed lines as plotted in Fig. 3.

Based on the law of momentum conservation and the above double-Gaussian distribution with the self-similarity assumption, Keane et al. [25] and Schreiber et al. [26] derived the analytical solution for the streamwise function as follows,

$$F(x) = \frac{M - \sqrt{M^2 - 1/2N\,C_T D^2}}{2N} \tag{5}$$

where M and N are expressed as follows,

$$M = 2\sigma^2\exp\left(-\frac{r_{min}^2}{2\sigma^2}\right) + \sqrt{2\pi}\,r_{min}\sigma\mathrm{erf}\left(\frac{r_{min}}{\sqrt{2}\sigma}\right) \tag{6}$$

$$N = \sigma^2\exp\left(-\frac{r_{min}^2}{\sigma^2}\right) + \frac{\sqrt{\pi}}{2}r_{min}\sigma\mathrm{erf}\left(\frac{r_{min}}{\sigma}\right) \tag{7}$$

A momentum conserving solution of F in Eq. (5) exists only when

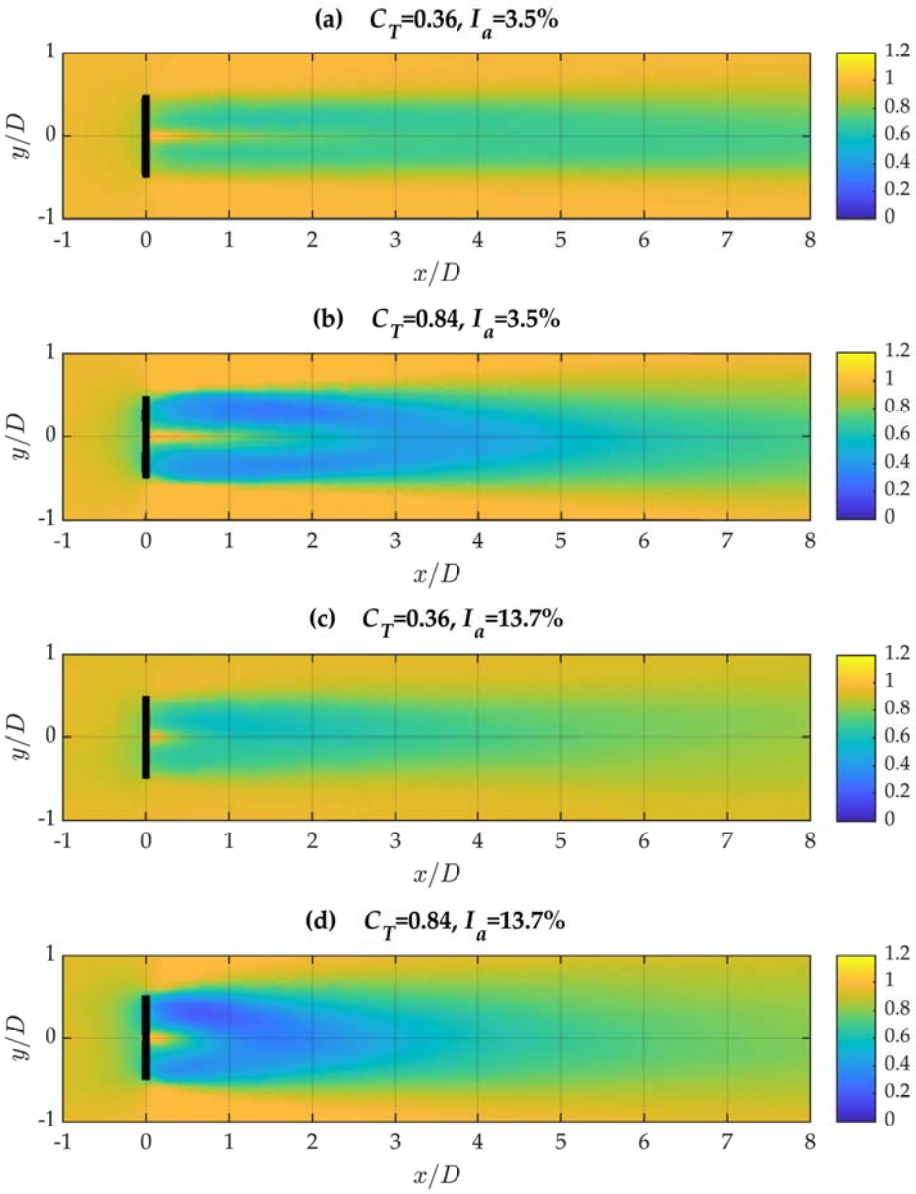

Fig. 1. Contours of mean streamwise velocity at the hub height obtained from LES simulations of a utility-scale wind turbine: (a) Case1 (C_T=0.36, I_a=3.5 %), (b) Case 2 (C_T=0.84, I_a=3.5 %), (c) Case 3 (C_T=0.36, I_a=13.7 %), (d) Case 4 (C_T=0.84, I_a=13.7 %).

$M^2 - 1/2N\,C_TD^2 > 0$, however, $M^2 - 1/2N\,C_TD^2$ can become negative in the near-wake region for large values of C_T. Therefore, a third order approximation of the Taylor expansion of Eq. (5) is performed to obtain a stable solution as shown in Eq. (8).

$$F(x) = \frac{M - \sqrt{M^2 - 1/2N\,C_TD^2}}{2N} \cong \frac{C_TD^2}{8M} + \frac{NC_T^2D^4}{64M^3} + \frac{N^2C_T^3D^6}{128M^5} \tag{8}$$

Note that the radial position of the Gaussian extrema r_{min} and the standard deviation of the Gaussian function σ have no analytical solutions and need to be modelled. In this study, r_{min} and σ are firstly fitted to the velocity profiles and illustrated as a function of normalized downwind distance for the different cases in Fig. 4 and Fig. 5, respectively. In the original formulation by Keane et al. [25] and Keane [27], r_{min}/R is set as fixed value close to 0.5 which is constant at different downwind locations, however, it can be seen from Fig. 4 that r_{min} decreases in the near-wake region and increases gradually in the far-wake region. The tipping point at which the r_{min} reaches minimum is around 4D for low turbulence cases and 2D for high turbulence cases. This is consistent with the phenomenon shown in Fig. 1, where the double-peak distribution transits to a single peak at a similar distance with the tipping point of r_{min}. Based on the characteristics described above, a formula is proposed to fit the variation of r_{min} with the downwind distance x.

$$\frac{r_{min}}{R} = a\frac{x}{D} + b\left(1 + c\frac{x}{D}\right)^{-0.5} \tag{9}$$

where $R = D/2$, b represents the initial value of r_{min} at $x = 0$. The values of normalized Gaussian minimum r_{min}/R fitted by Eq. (9) are plotted by red lines in Fig. 4 for comparison as well, from which Eq. (9) can well describe the variation for different cases.

As for the modelling of σ, Keane [27] took it to be varying as x^n, where n is the exponent of downwind distance and needs to be tuned for different conditions. As shown in Fig. 5, the σ of the double-Gaussian function expands approximately linearly for the different cases, where the red lines represent the linear fitting curves for the normalized values of σ/D. It is known that approximating the normalized standard deviation of the velocity deficit profile with a linear expression in high turbulence conditions may not be very accurate. Proposing a reasonable

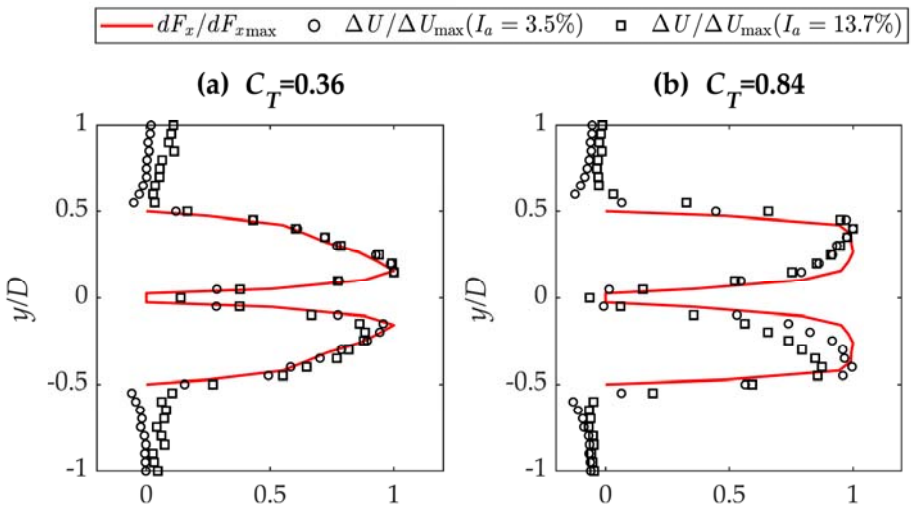

Fig. 2. Horizontal distribution of normalized velocity deficit at $x = 0.2D$ and normalized thrust force on the rotor. (a) C_T=0.36, (b) C_T=0.84.

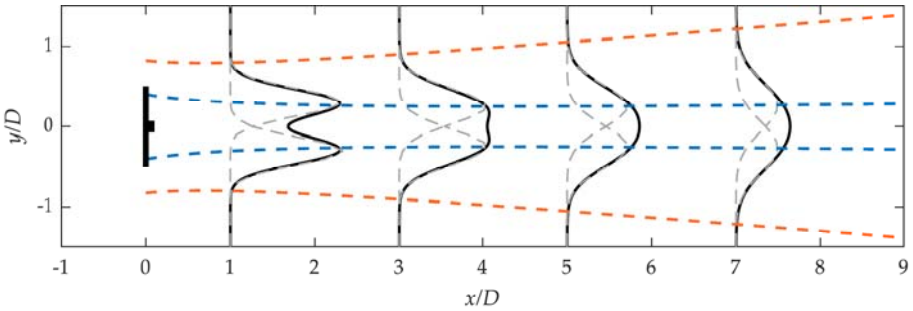

Fig. 3. Schematic of the double-Gaussian full wake model: The double-Gaussian and its constituent single-Gaussian functions are plotted as black solid and gray dashed lines, respectively. Blue dashed and orange dashed lines represent the location of the Gaussian extrema r_{min} and the wake boundary, respectively. (For interpretation of the references to colour in this figure legend, the reader is referred to the web version of this article.)

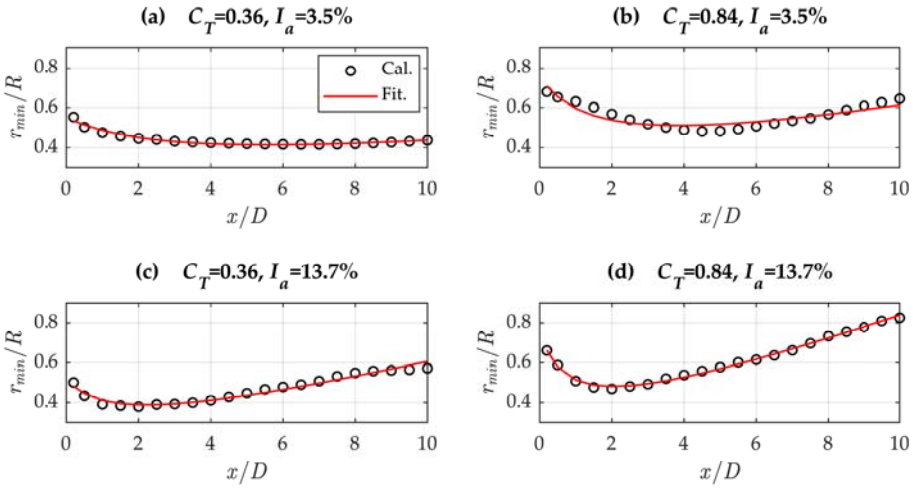

Fig. 4. Normalized Gaussian minimum of the velocity deficit profiles: (a) Case1 (C_T=0.36, I_a=3.5 %), (b) Case 2 (C_T=0.84, I_a=3.5 %), (c) Case 3 (C_T=0.36, I_a=13.7 %), (d) Case 4 (C_T=0.84, I_a=13.7 %). Red lines represent the values fitted to Eq. (9). (For interpretation of the references to colour in this figure legend, the reader is referred to the web version of this article.)

nonlinear expression for high turbulence cases remains a future work. Using the same formula for all cases allows us to maintain a consistent model expression across all cases. Therefore, σ is formulated with a linear function as follows,

$$\frac{\sigma}{D} = k^* \frac{x}{D} + \varepsilon \tag{10}$$

where k^* governs the rate of wake expansion or wake deficit recovery, and ε denotes the initial wake expansion at $x = 0$. Note that although the

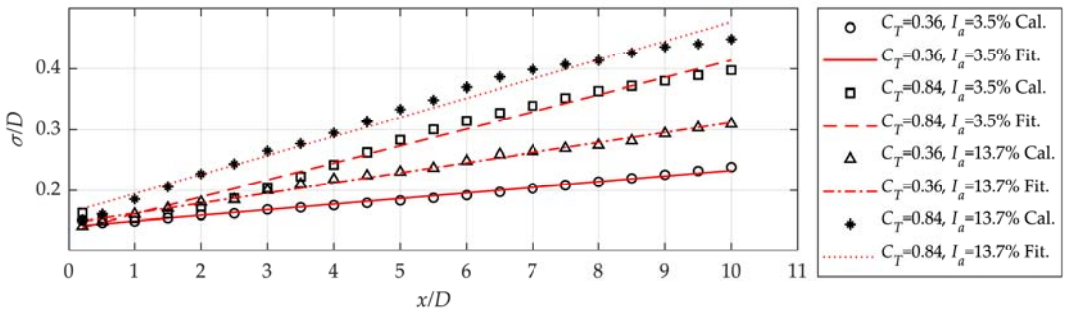

Fig. 5. Normalized standard deviation of the velocity deficit profiles: (a) Case 1 (C_T=0.36, I_a=3.5 %), (b) Case 2 (C_T=0.84, I_a=3.5 %), (c) Case 3 (C_T=0.36, I_a=13.7 %), (d) Case 4 (C_T=0.84, I_a=13.7 %). Red lines represent the values fitted to Eq. (10). (For interpretation of the references to colour in this figure legend, the reader is referred to the web version of this article.)

wake expansion for double-Gaussian velocity deficits is also assumed to be linear in the previous study by Schreiber et al. [26], the current study is first time to demonstrate it and identify the model parameters. The plots in Fig. 5 illustrate that the wake expands faster as the ambient turbulence intensity increases. It is because the higher surrounding turbulence enhances flow mixing, resulting in faster wake expansion and recovery. The wake expansion rate is likely to be more influenced by the turbine than the ambient turbulence. This inference can also be seen if the small C_T cases and large C_T cases with same I_a are compared, where the wake width of large C_T cases increase faster that of small C_T cases. These characteristics imply that wake behavior depends on not only the ambient turbulence but also the turbine thrust coefficient.

In the above two new formulas, there are five unknown parameters in Eqs. (9) and (10), including a, b, c, k^* and ε. In the original formula. Regarding to ε, Schreiber et al. [26] derived it based on mass conservation; however, the solution can only be calculated numerically as a function of the thrust coefficient C_T and the Gaussian minimum $r_{\min}$. To generalize the model for different turbulence conditions and turbine operations, the above five unknown parameters including a, b, c, k^* and ε are modelled as the function of the thrust coefficient C_T and the turbulence intensity I_a as follows,

$$\kappa = C_1 C_T^{C_2} I_a^{C_3} \tag{11}$$

This empirical formula was originally developed by Ishihara and Qian [14], which can give the model greater tuning abilities by considering the inflow flow and turbine operating conditions with three empirical constants of C_1, C_2 and C_3. To obtain the values of empirical constants for above five model parameters, an error-minimization optimization is utilized to process the entire data set concurrently, where the error is defined as follows,

$$\text{error} = \sqrt{\sum_{i=1}^{N} \text{RMSE}_i} \tag{12}$$

It describes the root-sum-square of the RMSE_i considering $N = 4$ cases with different conditions as shown in Table 3. The RMSE denotes the root-mean-squared-error between the wake model and LES data. The performance of the wake model depends on the data adopted for its parameter identification, thus, the LES data from $x = 0.5D$ to $10D$ at intervals of $0.5D$ are used for accurately gauging not only the position of the velocity deficit minimum but also the wake width expansion rate. The genetic algorithm (GA) optimization tool in MATLAB [38], is adopted to identify the empirical constants in the above formulas. After the error-optimization process, the empirical constants are identified and the expression for a, b, c, k^* and ε are summarized as follows. The model parameters are identified based on cases where the ambient turbulence intensity I_a is larger than 0.03, therefore, in engineering applications, I_a should be set to 0.03 when the ambient turbulence intensity is less than 0.03.

$$a = 0.2C_T^{0.49} I_a^{0.5} \tag{13}$$

$$b = 0.75C_T^{0.53} I_a^{-0.05} \tag{14}$$

Table 3
Description of the Ishihara-Qian DG model.

Wake model	Formulas	Parameters
Wake width	$\frac{\sigma}{D} = k^*\frac{x}{D} + \varepsilon^*, D_w = 2r_{\min} + 4\sqrt{2\ln 2}\sigma$	$k^* = 0.09C_T^{1.14} I_a^{0.32}$, $\varepsilon = 0.15C_T^{-0.02} I_a^{0.02}$
Velocity deficit	$\Delta U(x,y,z)/U_h = \left(\frac{C_T D^2}{8M} + \frac{NC_T^2 D^4}{64M^3} + \frac{N^2 C_T^3 D^6}{128M^5}\right)\frac{1}{2}\left\{\exp\left(-\frac{(r+r_{min})^2}{2\sigma^2}\right) + \exp\left(-\frac{(r-r_{min})^2}{2\sigma^2}\right)\right\}$ $M = 2\sigma^2\exp\left(-\frac{r_{min}^2}{2\sigma^2}\right) + \sqrt{2\pi}\, r_{min}\sigma\,\text{erf}\left(\frac{r_{min}}{\sqrt{2}\,\sigma}\right)$ $N = \sigma^2\exp\left(-\frac{r_{min}^2}{\sigma^2}\right) + \frac{\sqrt{\pi}}{2} r_{min}\sigma\,\text{erf}\left(\frac{r_{min}}{\sigma}\right)$ $\frac{r_{min}}{D/2} = a\frac{x}{D} + b\left(1 + c\frac{x}{D}\right)^{-0.5}$ $r = \sqrt{y^2 + (z-H)^2}$	$a = 0.2C_T^{0.49} I_a^{0.5}$, $b = 0.75C_T^{0.53} I_a^{-0.05}$, $c = 5.86C_T^{1.1} I_a^{0.47}$
Added turbulence	$\Delta\sigma_u(x,y,z)/U_h = \frac{1}{d + e{\cdot}x/D + f(1 + x/D)^{-2}}$ $\bullet\left\{k_1\exp\left(-\frac{(r-D/2)^2}{2\sigma^2}\right) + k_2\exp\left(-\frac{(r+D/2)^2}{2\sigma^2}\right)\right\} - \Delta I_a(y,z)$ $\Delta I_a(y,z) = \begin{cases} 0 \; else \\ I_a\sin^2\left(\pi\frac{H-z}{D}\right)\cos^2\left(\pi\frac{y}{D}\right) \; (z < H, \lvert y\rvert \le D) \end{cases}$	$d = 2.3C_T^{-1.2}, e = 1.0I_a^{0.1}, f = 0.7C_T^{-3.2} I_a^{-0.45}$ $k_1 = \begin{cases} \cos^2(\pi/2{\cdot}(r/D - 0.5)) & r/D \le 0.5 \\ 1 & r/D > 0.5 \end{cases}$ $k_2 = \begin{cases} \cos^2(\pi/2{\cdot}(r/D + 0.5)) & r/D \le 0.5 \\ 0 & r/D > 0.5 \end{cases}$

$$c = 5.86 C_T^{1.1} I_a^{0.47} \tag{15}$$

$$k^* = 0.09 C_T^{1.14} I_a^{0.32} \tag{16}$$

$$\varepsilon = 0.15 C_T^{-0.02} I_a^{0.02} \tag{17}$$

Note that, the model for the added turbulence intensity proposed by Ishihara and Qian [14], which is also a double-Gaussian model describing the three-dimensional distribution of turbine generated turbulence intensity in the wake, is used in couple with the current version of model for velocity deficit. To facilitate the implementation of the newly proposed model, Table 3 summarizes the Ishihara-Qian model with double-Gaussian distributions (hereafter referred to as Ishihara-Qian DG model), where the key formulars and parameters are listed. In addition, the wake model for wind turbine towers proposed by Yoshida and Kiyoki [39] can be combined with the newly proposed wake model for a wider range of engineering applications.

3. Model validation

To validate the novel full wake model, the results predicted by the newly proposed model are compared against the LES data and experimental data for the scenario of single wind turbine wake in Section 3.1. Subsequently, Section 3.2 presents the comparison between the wake models and LES data regarding the power production in wind farms for the scenario of multiple wind turbine wakes.

3.1. Single wind turbine wake

Fig. 6 plots the horizontal distributions of normalized velocity deficit at several downwind locations to represent the quantitative comparison between different wake models and the numerical results. From an engineering point of view, it is not possible to place two turbines closer than 1D, so values below $x/D < 1$ are not included in Fig. 6. Open circles depict the LES data as presented in Section 2.1. The blue, yellow, green and red lines illustrate the predicted results by Ishihara and Qian's

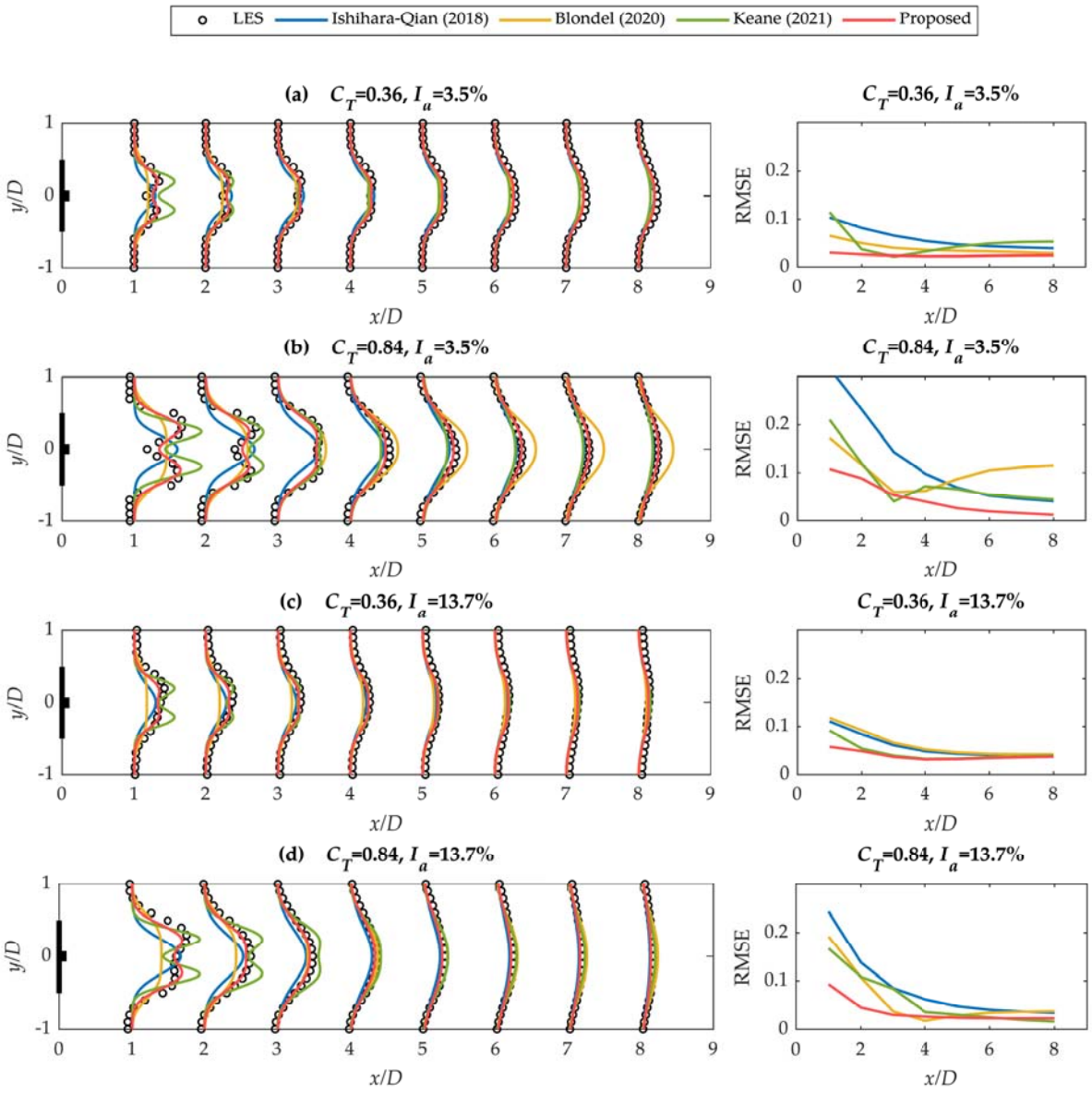

Fig. 6. Horizontal profiles of normalized velocity deficit (left) and corresponding RMSEs of different wake models (right) at various downstream locations in wind turbine wakes: (a) Case1 (C_T=0.36, I_a=3.5 %), (b) Case 2 (C_T=0.84, I_a=3.5 %), (c) Case 3 (C_T=0.36, I_a=13.7 %), (d) Case 4 (C_T=0.84, I_a=13.7 %).

single-Gaussian model [14] (hereafter referred to as "Ishihara-Qian SG model"), Blondel's super-Gaussian model [22], and Keane's conventional double-Gaussian wake model [27] and the newly proposed full wake model. This study focusses on model performance not only in the near wake region but also in the far wake region and demonstrates the advancement of the new model in the far wake region, compared with the Ishihara and Qian single-Gaussian model [14]. For the Blondel's super-Gaussian model, the default model parameters from reference [22] are used. The ratio of effective rotor diameter d_e/d_0 and wake expansion exponent n in Keane's model are set as 1, which are consistent with the proposed model in this study. The other two parameters in Keane's model including wake expansion rate k and local Gaussian minimum $r_{\min}$ are the values from the cases with the closest C_T in the reference [27]. The corresponding RMSEs with respect to the LES solutions are also reported at the right-hand side using same colour lines for each wake model. The normalized velocity deficit is expressed as:

$$\frac{\Delta U}{U_{0,h}} = \frac{U_{0,h} - U}{U_{0,h}} \tag{18}$$

where $U_{0,h}$ is the inflow velocity at the hub height, U is the streamwise velocity, and ΔU is the velocity deficit. The x-axis denotes the distance from the wind turbine and is normalized by the rotor diameter D. It is noted from the LES data plotted in Fig. 6 that, for low ambient turbulence cases, the velocity deficit presents a transition from double-Gaussian distribution in the near-wake region ($x < 3D$) to a smooth top-hat or an approximate super-Gaussian shape in mid-wake region ($x = 3D \sim 5D$) and finally to a single-Gaussian distribution in the far-wake region ($x > 5D$). While for high ambient turbulence case, because of the stronger turbulent mixing, the double-Gaussian distribution can only be clearly visible in the near-wake region ($x < 2D$) and then develops to single-Gaussian shape very quickly. In general, the velocity deficit profiles predicted by the proposed full wake model capture these behaviors very well and show most favorable agreement with the LES data. Note that the calibration of the model parameters is performed with the goal of minimizing the overall errors of the four cases, but this does not guarantee that the obtained parameters are optimal for each case. Therefore, the differences with LES data may not be sufficiently suppressed in some locations. As anticipated, the Ishihara-Qian SG model shows a very large RMSE in the near-wake region than the other two double-Gaussian models, but it still can provide good performance in the far-wake region where the velocity deficit distributions are indeed characterized by one peak. Compared with the

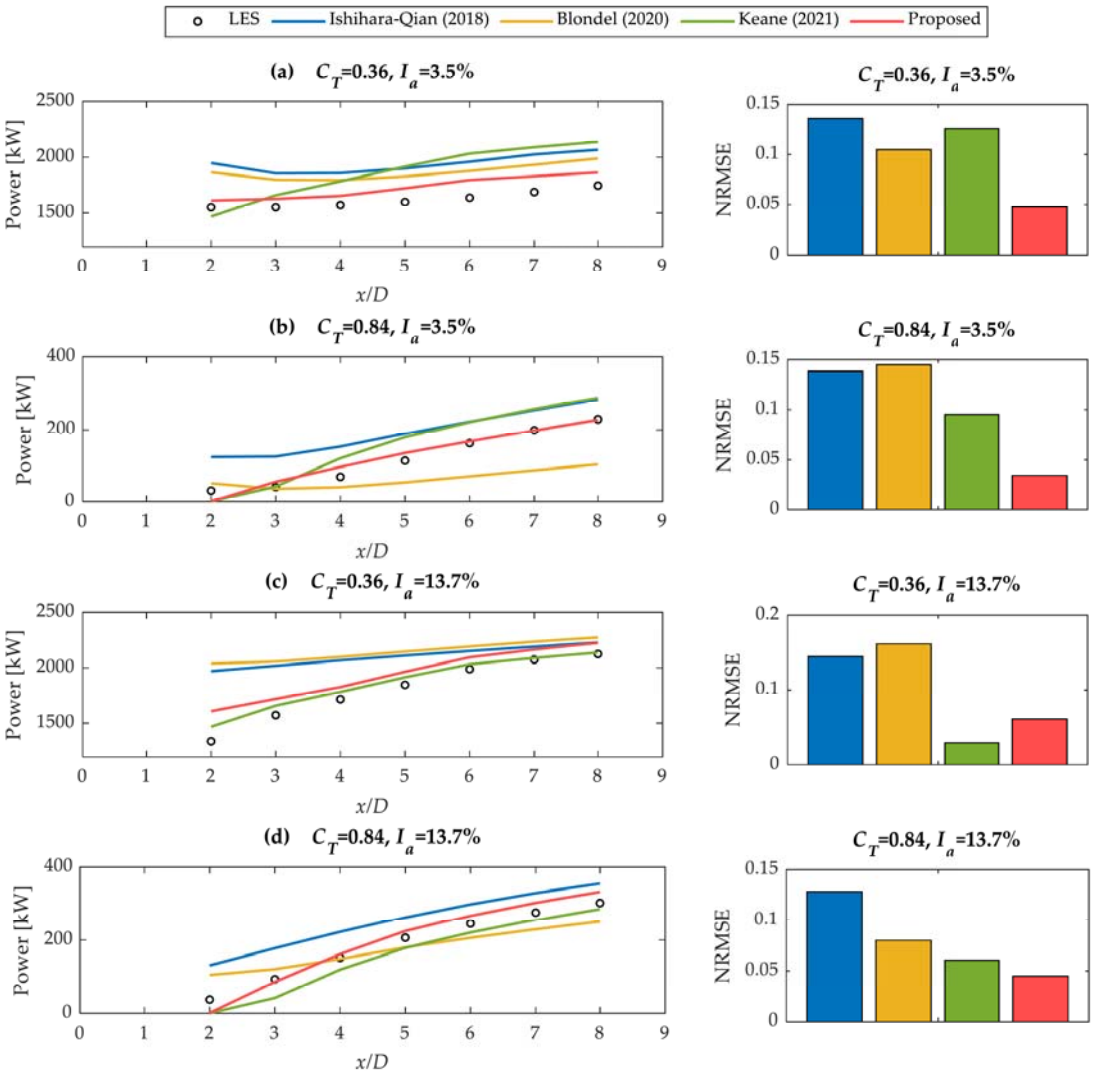

Fig. 7. Variation of wind power generated by the turbine located at different downwind locations: (a) Case1 (C_T=0.36, I_a=3.5 %), (b) Case 2 (C_T=0.84, I_a=3.5 %), (c) Case 3 (C_T=0.36, I_a=13.7 %), (d) Case 4 ((C_T=0.84, I_a=13.7 %).

single-Gaussian model, the Blondel's super-Gaussian model can capture a wider wake width in the near wake region, but it generally underestimates the velocity deficit in the near wake region. In the far wake region, the performance of the super-Gaussian model is generally satisfactory, except for a significant overestimation in Case 3. The Keane model overestimates the velocity deficits in the near-wake region ($x = 1D \sim 2D$) for all cases, and underestimates those in the far-wake region for small C_T cases. These discrepancies can be attributed to the fact that the Gaussian minimum $r_{\min}$ is set to be constant in different downwind distances and the wake expansion rate k is not variable with ambient turbulence intensity.

Next, the ability of the above three wake models to predict the power production of another turbine placed in the wake region is investigated. Firstly, the rotor-effective incoming wind speed U_e for the turbine experiencing wakes is defined as:

$$U_e = \sqrt[3]{\frac{\int_{A_0} U_w^3 \mathrm{dA}}{A_0}} \tag{19}$$

where U_w is the wind speed in the wake region, A_0 is the rotor area. The power curve of the MHI 2.4 MW turbine as described in Qian et al. [20] is used to estimate the power generated by a wind turbine located at different downwind locations for the four cases as plotted in Fig. 7, where the open circles denote the power obtained by the LES, and those predicted by three wake models are shown by blue, green and red lines, respectively. Here, only the power at locations of $x \geq 2D$ are evaluated considering that a wind turbine is rarely located in the region of $x < 2D$. The proposed full wake model reasonably predicts the variation of power versus downwind locations for all cases. The Ishihara-Qian SG model generally overestimates power, especially in the near-wake region due to the assumption of the single-Gaussian distribution, which leads to the underestimation of velocity deficit in the wake region as plotted in Fig. 6. Blondel's super-Gaussian model overestimates the power in the mid- and far-wake regions when C_T is small, while underestimates them when C_T is large. Keane's model overestimates the power in the mid- and far-wake regions for the two low turbulence cases and slightly underestimates it for Case 4 with high turbulence and large thrust coefficient. Additionally, the corresponding NRMSEs with respect LES results are plotted as well at the right-hand side of each figure, where the NRMSE denotes the RMSE of predicted power of downwind turbine normalized by the LES resolved power of upwind turbine. The proposed model consistently has the lowest NRMSE and high accuracy across all conditions. In Case 3 (C_T=0.36, I_a=13.7 %), the error of the proposed model is slightly higher than that of Keane's model, but the proposed model shows a steady improvement in accuracy in almost all cases, and the total NRMSE of the proposed model for the four cases is about half of that of the Keane's model.

To further validate the accuracy of the proposed model, four more data sets are utilized and the relevant information regarding turbines size, operation, inflow and data type for each case is summarized in Table 4. The first data set for Case V1 is from the wind tunnel experiment performed with the scaled wind turbine G1 [26], where the horizontal time-averaged velocity profiles at six selected downstream locations (x/D = 1.4, 1.7, 2, 3, 4, and 6) were measured in the wind tunnel of the Politecnico di Milano. For Case V2, horizontal profiles of normalized velocity at three selected downwind locations (x/D = 1, 3, and 4) of a MHI 2.4 MW offshore wind turbine at Choshi site were obtained from a scanning LiDAR in PPI scan mode [40]. Since the LiDAR scan azimuth angle is almost perpendicular to the incoming flow for x ≈ 2D, the measured data is not plotted at this location due to the large measurement error. The third data set for Case V3 corresponds to two vertical profiles selected in the near wake region of a UP77 1.5 MW onshore wind turbine located in northern Hebei Province, China [41], measured by a scanning LiDAR in RHI scan mode. The last data set for Case V4 is taken from the research data in the CL-Windcon project [42], a Large Eddy Simulation (LES) of the wakes of a INNWIND.EU 10 MW reference turbine using the high-fidelity solver SOWFA. This selected data set, characterized by low incoming turbulence intensity, was representative of offshore environments. Vertical profiles of streamwise velocity were sampled at six selected locations (x/D = 1.5, 2, 2.5, 3, 4, and 6) downstream of the wind turbine. As shown in previous research by Ishihara and Qian [14], wake characteristics such as mean velocity deficit and added turbulence intensity of the model wind turbine and the utility-scale turbine are relatively close if thrust coefficient and ambient turbulence intensity are the same. Therefore, although the wind turbines in the first three validation cases are not very large, they are able to validate the accuracy of the proposed model.

To illustrate a quantitative comparison of the predicted results by the wake models with reference data sets, the horizontal and vertical profiles of time-averaged velocity at selected downwind locations are plotted in Fig. 8, Fig. 9, Fig. 10, and Fig. 11 for the four validation cases, respectively. Here, all values are normalized by the incoming wind speed U_0. The results predicted by the proposed wake model, the super-Gaussian model, the Keane's model and the Ishihara-Qian SG model are plotted using red, yellow, green and blue lines, respectively. Compared with the super-Gaussian and single-Gaussian models, it is found that the wake profiles estimated by the proposed double-Gaussian model show good agreement with those obtained from the reference data sets. The parameters of the proposed wake model are not calibrated using these three experimental data and one numerical data. This indicates that the proposed wake model is robust enough to predict both horizontal and vertical profiles in the wake of wind turbines with different sizes under different operating conditions and environment conditions. However, Keane's model clearly underestimates the minimum wind speeds in the near wake-region ($x < 2D$). This is likely due to the use of a non-physical solution in Eq. (5). Furthermore, the locations of the minima in the Gaussian distribution do not match well the measurement, which also leads to discrepancies in far wake region.

3.2. Wind farm power production

To apply the proposed double-Gaussian wake models to a wind farm power prediction, the multiple wake model proposed by Qian and Ishihara [43] are utilized. As summarized in Table 5, the multiple wake model includes the formulas of the rotor onset wind speed $U_{h,i}$, turbulence intensity $I_{a,i}$, rotor-based energy deficit superposition principle, and a modified Linear Sum of Square (LSS) principle for turbulence intensity. The detailed implementation of the multiple wake model is used as shown in Qian and Ishihara [43].

The dataset of LES results [44] for the Horns Rev offshore wind farm is selected for validation, where 80 Vestas 2 MW wind turbines are

Table 4
Cases for model validation.

Case	Turbine	D (m)	H (m)	C_T	I_a	Wake profile	Reference data type
V1	G1 [26]	1.1	0.8	0.36	3.5 %	Horizontal	Wind tunnel experiment
V2	MHI 2.4 MW [40]	92	80	0.84	3.5 %	Horizontal	Scanning LiDAR
V3	UP77 1.5 MW [41]	77	65	0.72	11 %	Vertical	Scanning LiDAR
V4	INNWIND.EU 10 MW [42]	178.3	119	0.84	5.1 %	Vertical	LES simulation by SOWFA

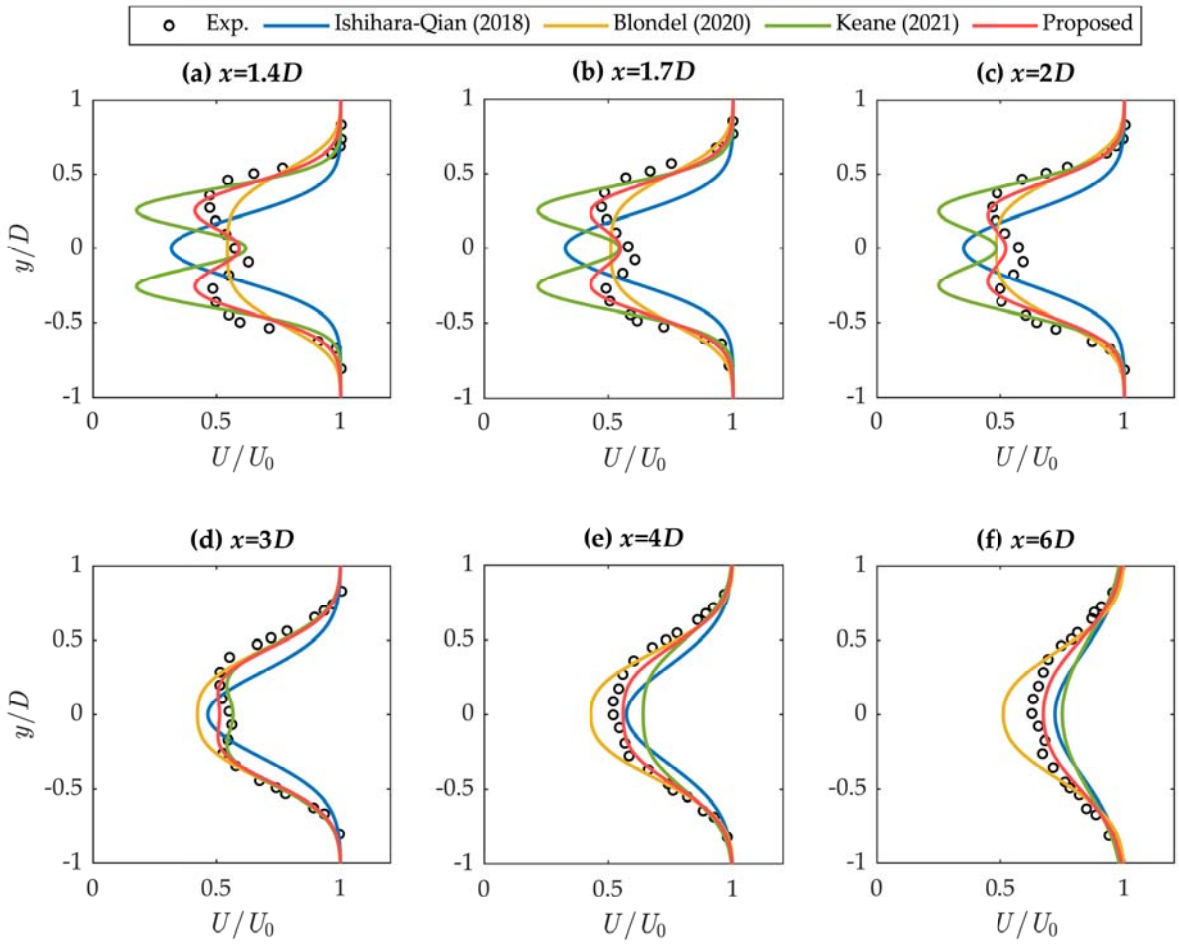

Fig. 8. Validation of the proposed model using the horizontal profiles of mean streamwise velocity at hub height from the wind tunnel tests of a G1 wind turbine [26].

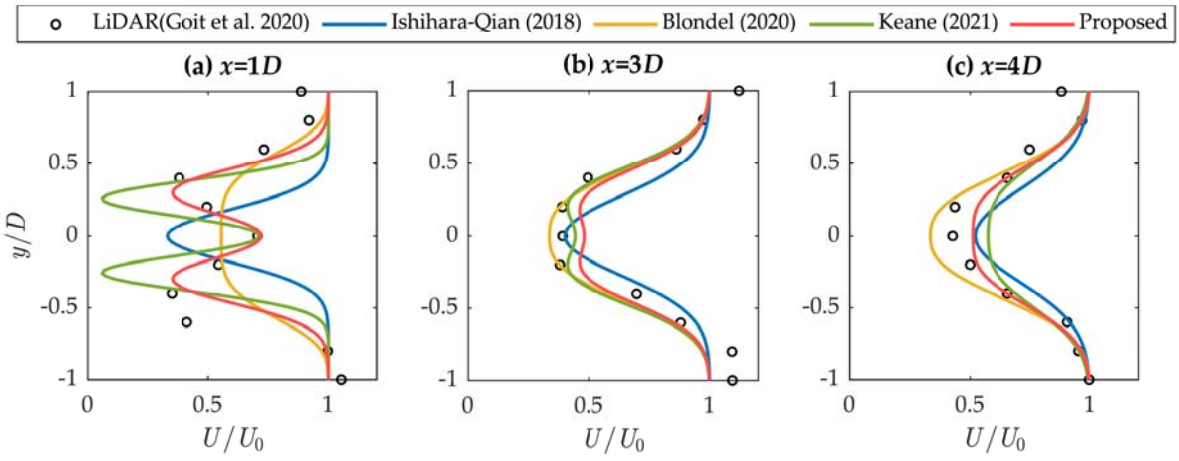

Fig. 9. Validation of the proposed model using the horizontal profiles of mean streamwise velocity at hub height from the scanning LiDAR measurements of a 2.4 MW MHI offshore wind turbine at Choshi site [40].

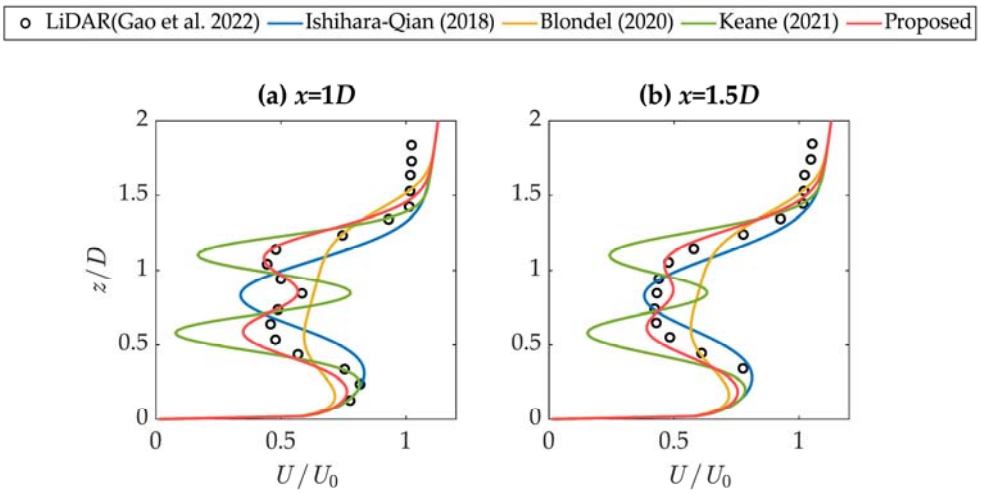

Fig. 10. Validation of the proposed model using the vertical profiles of mean streamwise velocity at the central cross section from the scanning LiDAR measurements of a 1.5 MW UP77 onshore wind turbine [41].

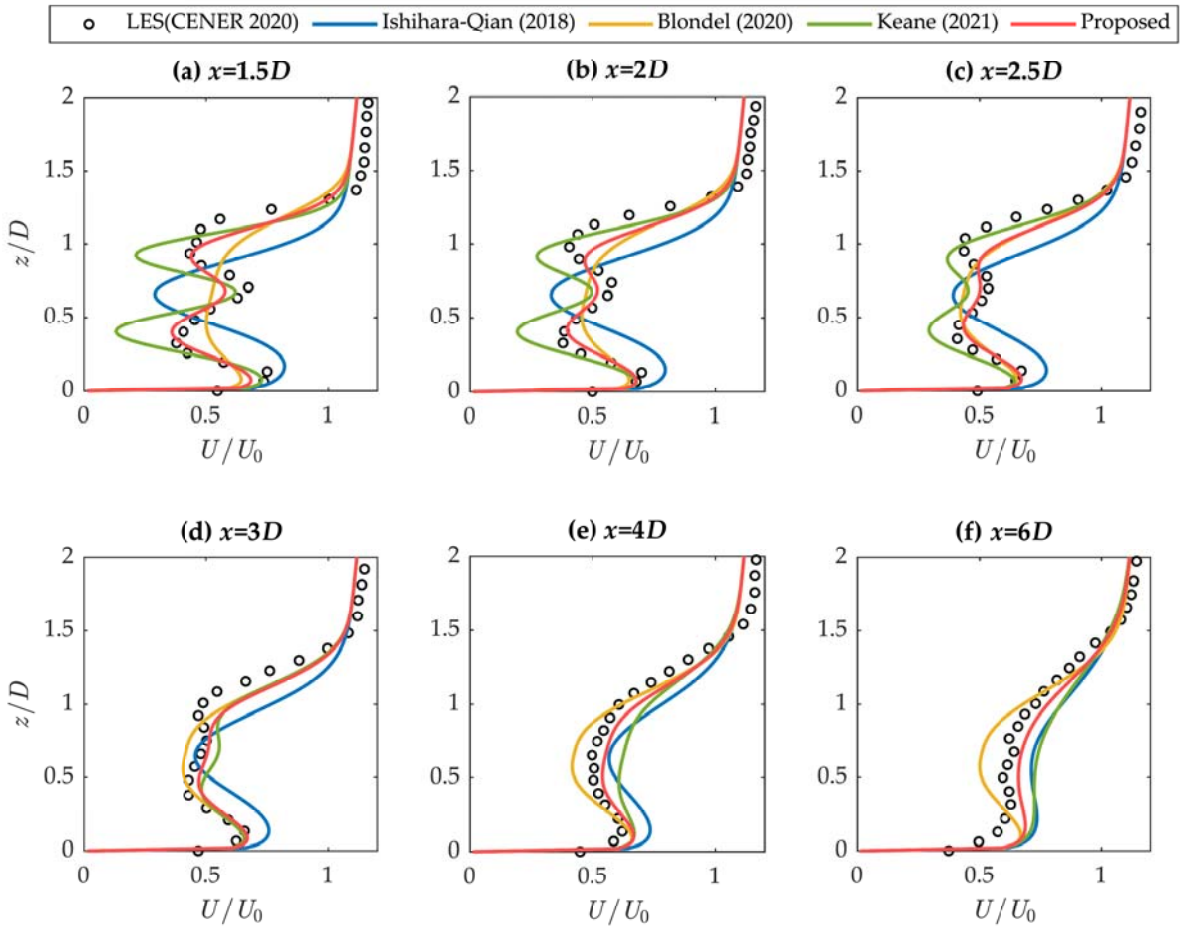

Fig. 11. Validation of the proposed model using the vertical profiles of mean streamwise velocity the central cross section from high-fidelity SOWFA simulation of a 10 MW INNWIND.EU reference wind turbine [42].

Table 5
Description of the multiple wake model.

Wake model	Formulas
Rotor onset	Equivalent wind speed: $U_{h,i} = \frac{1}{A}\int_{rotor} U(x_i, y, z)dA$ Equivalent turbulence intensity: $I_{a,i} = \frac{1}{AU_{h,i}}\sqrt{\int_{rotor}\sigma_u^2(x_i, y, z)dA}$
Velocity deficit superposition	$U = \sqrt{U_0^2 - \sum_{i=1}^{n}\left(U_{h,i}^2 - U_{w,i}^2\right)}$, $U_{w,i} = U_{h,i} - \Delta U_i$, $\Delta U_i/U_{h,i} = F(C_{T,i}, I_{a,i}, x/D)\phi(r_i/\sigma_i)$
Added turbulence superposition	$\sigma_u^2 = \sigma_{u,0}^2 + \sum_{i=1}^{n}\left(\Delta\sigma_{u,i} + \Delta\sigma_{u,ij}\right)^2$, $\Delta\sigma_{u,i}/U_{h,i} = G(C_{T,i}, I_{a,i}, x/D)\varphi(r_i/\sigma_i)$

arranged as shown in Fig. 9 (a). There are 10 columns running east-west and 8 rows running north-south. Three typical wind directions as noted by the solid arrows in Fig. 9 (a) are simulated, where turbines are in a full overlap wake condition. The corresponding turbine distances and free stream incoming wind conditions are listed in Table 6.

For quantitative comparison, Fig. 12 illustrates the predicted power production in the three wind directions, where the power of each wind turbine is normalized by the most upstream one. The comparison of wind farm power in a wider range of wind direction is presented in Fig. 12 as well, where the simulated power output is normalized by the power of an equivalent number of stand-alone wind turbines operating in the same incoming wind condition. For comparison, the predicted powers by the Ishihara-Qian SG model, Blondel's model, Keane's model and proposed model are plotted by the blue lines, yellow lines, green lines and red lines, respectively. Seen from the LES results plotted by open circles in Fig. 12, the second downstream turbine produces significantly less power, while the reduction in further downstream turbines subsides. This is because the relatively higher turbulence levels in the wake compared with the incoming flow increase flow entrainment, resulting in faster wake recovery. The proposed wake model illustrates favorable agreement with the LES data for different wind directions. The Ishihara-Qian SG model generally overestimates the powers of downstream turbines, while the Blondel' super-Gaussian model presents significant underestimations for all the cases. The Keane's model gives visible underestimations, especially when the wind direction is within $270^\circ \pm 5^\circ$, which can be seen more clearly in Fig. 13. The Keane's model is not turbulence intensity dependent, thus it cannot consider the increase of turbulence intensity in the wind farm. The maximum relative error of predicted power with respect to LES data is also estimated for each case and summarized in Table 7. The proposed model shows smaller errors for each wind direction than the Ishihara-Qian single-Gaussian model and provides good agreement with the LES data. It is noticed that the maximum error predicted by Blondel's super-Gaussian model generally occurs in the second row, which means that the main discrepancy derives from the original single wake model, respectively. The Keane's double Gaussian model exhibits an increase in errors as the number of turbine rows grows.

Table 6
Description of simulation cases for the Horns Rev. offshore wind farm.

Simulation Case	Wind direction	Turbine distance	Free stream wind speed at hub height	Ambient turbulence intensity at hub height
Case 1	$\theta_{wind} = 270^\circ$	7.0 D	8 m/s	7.7 %
Case 2	$\theta_{wind} = 222^\circ$	9.3 D		
Case 3	$\theta_{wind} = 312^\circ$	10.4 D		

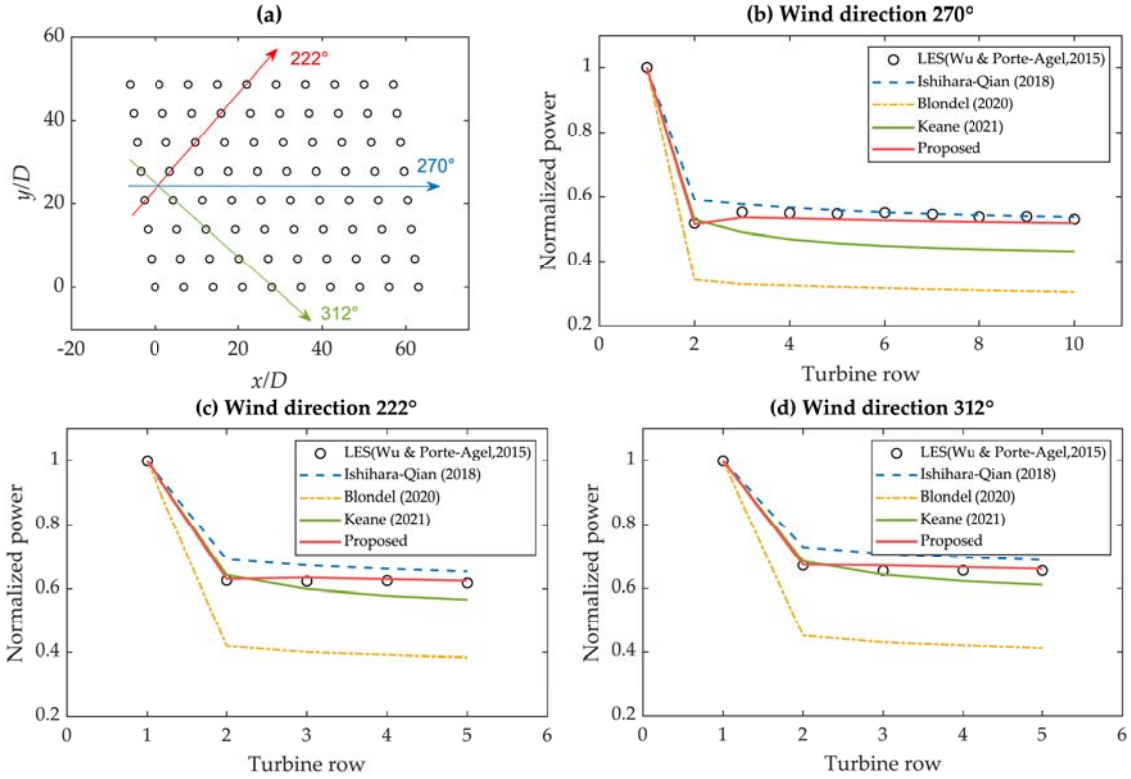

Fig. 12. Comparison of normalized power between LES data [44] and those predicted by wake models: (a) is the layout configuration of the Horns Rev. wind farm, and (b), (c), and (d) are results in wind directions of 270°, 222° and 312°, respectively.

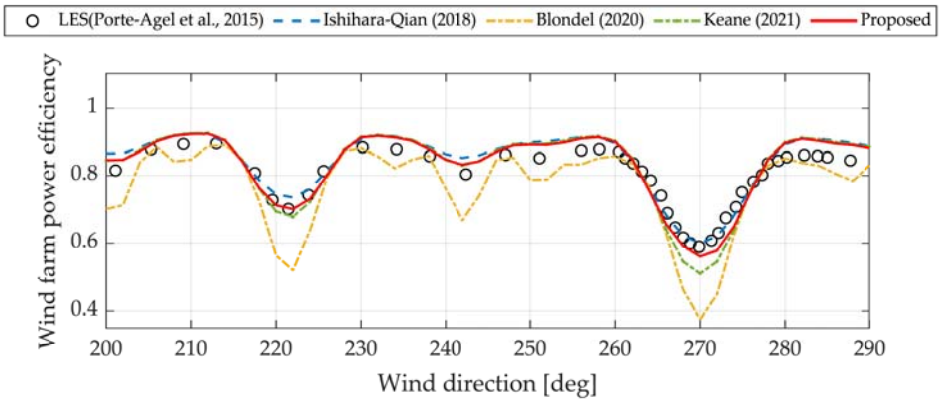

Fig. 13. Comparison of wind farm power efficiency of LES simulations [44] and wake model prediction for wind directions between 200° and 290°.

Table 7
Maximum relative error of predicted power with respect to measured data.

Model	$\theta_{wind} = 270^{\circ}$	$\theta_{wind} = 222^{\circ}$	$\theta_{wind} = 312^{\circ}$
Ishihara-Qian [14] – Single-Gaussian	11.8 %	10.5 %	8.4 %
Blondel [22] – Super-Gaussian	44.3 %	37.7 %	37.2 %
Keane [27] – Double-Gaussian	20.8 %	8.2 %	6.7 %
Proposed model – Double-Gaussian	4.3 %	1.9 %	2.6 %

4. Conclusions

In this study, a novel double-Gaussian full wake model is developed considering dependence on the ambient turbulence intensity and the thrust coefficient. The proposed wake model is then applied to power prediction in both scenarios of single wake and multiple wakes in a wind farm. The following conclusions are obtained:

1. The numerical results obtained from a series of LES simulations of a utility-scale wind turbine wake reveal that the double-peak distribution of velocity deficit in the near-wake is attributed to the ununiform distributed thrust force on the rotor. The ambient turbulence intensity and thrust coefficient are the key parameters that determine the wake recovery rate and the distance where double-peak velocity deficits transition to one-peak shape.
2. A novel full wake model using double-Gaussian function is derived to predict turbine wakes, where a non-divergent form for the amplitude of the velocity deficit in the streamwise direction is proposed using a third-order Taylor series approximation of the conventional formula. Compared to conventional models, a linear wake expansion rate and non-linear Gaussian minima are proposed to describe the shape transition of velocity deficit from the near-wake region to the far-wake region. All parameters of the proposed model are expressed as functions of the ambient turbulence and thrust coefficient to achieve better accuracy and robustness in practical applications.
3. In the single wake scenario, the velocity profiles estimated by the proposed wake model are in good agreement with those obtained from numerical simulations by LES and the measurements with different ambient turbulence and thrust coefficients conditions. Furthermore, comparison with the LES simulations of the Horns Rev wind farm reveals that the power predicted by the proposed wake model is accurate in multiple wake scenario with different turbine distances.

Author Contribution

This study was done by Guo-Wei Qian and Takeshi Ishihara. Guo-Wei Qian and Takeshi Ishihara designed the structure of the paper and wrote the paper.

CRediT authorship contribution statement

Guo-Wei Qian: Writing – original draft, Visualization, Software, Investigation, Formal analysis, Data curation. **Takeshi Ishihara:** Writing – review & editing, Validation, Supervision, Resources, Methodology, Conceptualization.

Declaration of competing interest

The authors declare that they have no known competing financial interests or personal relationships that could have appeared to influence the work reported in this paper.

Acknowledgments

This research was carried out as a part of the joint program for next generation of energy infrastructure with Toshiba Energy Systems & Solutions Corporation, J-POWER, Shimizu Corporation, MHI Vestas Offshore Wind Japan, ClassNK. This research was also supported by Guangdong Basic and Applied Basic Research Foundation (No. 2024A1515010547, No. 2024B1515250004), the National Key Research and Development Program of China (Grant No. 2022YFC2806300), the Innovation Group Project of Southern Marine Science and Engineering Guangdong Laboratory (Zhuhai) (No. 311023014), Fundamental Research Funds for the Central Universities, Sun Yat-sen University (Grant No. 23qnpy83). The authors express their deepest gratitude to the concerned parties for their assistance during this study.

Data availability

Data will be made available on request.

References

[1] WWEA. WWEA Annual Report 2023. https://wwindea.org/AnnualReport2023.. 2024. p. 1–10.
[2] Göçmen T, Van Der Laan P, Réthoré PE, Diaz AP, Larsen GC, Ott S. Wind turbine wake models developed at the technical university of Denmark: A review. Renew Sust Energ Rev 2016;60:752–69. https://doi.org/10.1016/j.rser.2016.01.113.
[3] Porté-Agel F, Bastankhah M, Shamsoddin S. Wind-turbine and wind-farm flows: A review. Bound-Layer Meteorol 2019;174:1–59. https://doi.org/10.1007/s10546-019-00473-0.
[4] Ishihara T, Yamaguchi A, Fujino Y. Development of a new wake model based on a wind tunnel experiment. Global Wind Power 2004.
[5] Crespo A, Hernández J, Frandsen S. Survey of modelling methods for wind turbine wakes and wind farms. Wind Energy 1999;2:1–24. https://doi.org/10.1002/(SICI)1099-1824(199901/03)2:1<1::AID-WE16>3.0.CO;2-7.
[6] Kheirabadi AC, Nagamune R. A quantitative review of wind farm control with the objective of wind farm power maximization. J Wind Eng Ind Aerodyn 2019;192:45–73. https://doi.org/10.1016/j.jweia.2019.06.015.
[7] Vermeer LJ, Sørensen JN, Crespo A. Wind turbine wake aerodynamics. Prog Aerosp Sci 2003;39:467–510. https://doi.org/10.1016/S0376-0421(03)00078-2.
[8] Crespo A, Hernández J. Turbulence characteristics in wind-turbine wakes. J Wind Eng Ind Aerodyn 1996;61:71–85. https://doi.org/10.1016/0167-6105(95)00033-X.
[9] Xie SB, Archer C. Self-similarity and turbulence characteristics of wind turbine wakes via large-eddy simulation. Wind Energy 2014;17:657–69. https://doi.org/10.1002/we.
[10] Jensen NO. A note on wind generator interaction. 1983. Riso-M-2411.
[11] Frandsen S, Barthelmie R, Pryor S, Rathmann O, Larsen S, Højstrup J. Analytical modelling of wind speed deficit in large offshore wind farms. Wind Energy 2006;9:39–53. https://doi.org/10.1002/we.
[12] Chamorro LP, Porte-Agel F. A wind-tunnel investigation of wind-turbine wakes: Boundary-layer turbulence effects. Bound-Layer Meteorol 2009;132:129–49. https://doi.org/10.1007/s10546-009-9380-8.
[13] Ainslie JF. Calculating the flowfield in the wake of wind turbines. J Wind Eng Ind Aerodyn 1988;27:213–24. https://doi.org/10.1016/0167-6105(88)90037-2.
[14] Ishihara T, Qian GW. A new Gaussian-based analytical wake model for wind turbines considering ambient turbulence intensities and thrust coefficient effects. J Wind Eng Ind Aerodyn 2018;177:275–92. https://doi.org/10.1016/j.jweia.2018.04.010.
[15] Gao X, Yang H, Lu L. Optimization of wind turbine layout position in a wind farm using a newly-developed two-dimensional wake model. Appl Energy 2016;174:192–200. https://doi.org/10.1016/j.apenergy.2016.04.098.
[16] Bastankhah M, Porté-Agel F. A new analytical model for wind-turbine wakes. Renew Energy 2014;70:116–23. https://doi.org/10.1016/j.renene.2014.01.002.
[17] Sun H, Yang H. Study on an innovative three-dimensional wind turbine wake model. Appl Energy 2018;226:483–93. https://doi.org/10.1016/J.APENERGY.2018.06.027.
[18] Sun H, Gao X, Yang H. Validations of three-dimensional wake models with the wind field measurements in complex terrain. Energy 2019;189:116213. https://doi.org/10.1016/j.energy.2019.116213.
[19] Gao X, Li B, Wang T, Sun H, Yang H, Li Y, et al. Investigation and validation of 3D wake model for horizontal-axis wind turbines based on filed measurements. Appl Energy 2020;260:114272. https://doi.org/10.1016/J.APENERGY.2019.114272.
[20] Qian GW, Song YP, Ishihara T. A control-oriented large eddy simulation of wind turbine wake considering effects of Coriolis force and time-varying wind conditions. Energy 2022;239:121876. https://doi.org/10.1016/j.energy.2021.121876.
[21] Schreiber J, Salbert B, Bottasso CL. Study of wind farm control potential based on SCADA data. J Phys Conf Ser 2018;1037:032012. https://doi.org/10.1088/1742-6596/1037/3/032012.
[22] Blondel F, Cathelain M. An alternative form of the super-Gaussian wind turbine wake model. Wind Energy Science 2020;5(9):1225–36. https://doi.org/10.5194/wes-5-1225-2020.
[23] Zhang S, Gao X, Lin J, Xu S, Zhu X, Sun H, et al. Discussion on the spatial-temporal inhomogeneity characteristic of horizontal-axis wind turbine's wake and improvement of four typical wake models. J Wind Eng Ind Aerodyn 2023;236:105368. https://doi.org/10.1016/j.jweia.2023.105368.
[24] Wei H, Zhao Z, Liu Y, Liu Y, Ali K, Liu H, et al. Development and validation of a three-dimensional wind-turbine wake model based on high-order Gaussian function. Ocean Eng 2024;312:119133. https://doi.org/10.1016/j.oceaneng.2024.119133.
[25] Keane A, Aguirre PEO, Ferchland H, Gallacher D. An analytical model for a full wind turbine wake. J Phys Conf Ser 2016;753:032039. https://doi.org/10.1088/1742-6596/753/3/032039.
[26] Schreiber J, Balbaa A, Bottasso CL. Brief communication: A double-Gaussian wake model. Wind Energy Science 2020;5:237–44. https://doi.org/10.5194/wes-5-237-2020.
[27] Keane A. Advancement of an analytical double-Gaussian full wind turbine wake model. Renew Energy 2021;171:687–708. https://doi.org/10.1016/j.renene.2021.02.078.
[28] Soesanto QMB, Yoshinaga T, Iida A. Anisotropic double-Gaussian analytical wake model for an isolated horizontal-axis wind turbine. Energy Sci Eng 2022;10:2123–45. https://doi.org/10.1002/ese3.1120.
[29] Zengler CP, Braunbehrens R, Tamaro S. Further improvements to the double-Gaussian wake model. J Phys Conf Ser 2024;2767:092066. https://doi.org/10.1088/1742-6596/2767/9/092066.
[30] Bourhis M, Buxton ORH. Influence of freestream turbulence and porosity on porous disk-generated wakes. Phys Rev Fluids 2024;9:124501. https://doi.org/10.1103/PhysRevFluids.9.124501.
[31] Vahidi D, Porté-Agel F. Influence of thrust coefficient on the wake of a wind turbine: A numerical and analytical study. Renew Energy 2025;240:122194. https://doi.org/10.1016/J.RENENE.2024.122194.
[32] Smagorinsky J. General circulation experiments with the primitive equations. Mon Weather Rev 1963;91:99–164. https://doi.org/10.1175/1520-0493(1963)091<0099:GCEWTP>2.3.CO;2.
[33] Fluent. ANSYS Fluent theory guide. Ansys Inc.; 2021.
[34] Burton T, Sharpe D, Jenkins N, Bossanyi E. Wind Energy Handbook. 2nd ed. Wiley; 2011.
[35] Foti D, Yang X, Shen L, Sotiropoulos F. Effect of wind turbine nacelle on turbine wake dynamics in large wind farms. J Fluid Mech 2019;869:1–26. https://doi.org/10.1017/jfm.2019.206.
[36] Abraham A, Dasari T, Hong J. Effect of turbine nacelle and tower on the near wake of a utility-scale wind turbine. J Wind Eng Ind Aerodyn 2019;193:103981. https://doi.org/10.1016/J.JWEIA.2019.103981.
[37] Neunaber I, Hölling M, Stevens RJAM, Schepers G, Peinke J. Distinct turbulent regions in the wake of a wind turbine and their inflow-dependent locations: The creation of a wake map. Energies 2020;13:5392. https://doi.org/10.3390/EN13205392.
[38] MATLAB. Inc. M. 2019.
[39] Yoshida S, Kiyoki S. Load equivalent tower shadow modeling for downwind turbines. Wind Energy (Japanese) 2007;31:77–85. https://doi.org/10.11333/JWEA1977.31.4_77.
[40] Goit JP, Yamaguchi A, Ishihara T. Measurement and prediction of wind fields at an offshore site by scanning doppler LiDAR and WRF. Atmosphere 2020;11(4):442. https://doi.org/10.3390/ATMOS11050442.
[41] Gao X, Zhang S, Li L, Xu S, Chen Y, Zhu X, et al. Quantification of 3D spatiotemporal inhomogeneity for wake characteristics with validations from field measurement and wind tunnel test. Energy 2022;254:124277. https://doi.org/10.1016/j.energy.2022.124277.
[42] CL-Windcon. Research Data. http://www.clwindcon.eu/research-data/; 2019. accessed on 13 February 2025.
[43] Qian GW, Ishihara T. Wind farm power maximization through wake steering with a new multiple wake model for prediction of turbulence intensity. Energy 2021;220:119680. https://doi.org/10.1016/j.energy.2020.119680.
[44] Wu YT, Porté-Agel F. Modeling turbine wakes and power losses within a wind farm using LES: An application to the Horns Rev offshore wind farm. Renew Energy 2015;75:945–55. https://doi.org/10.1016/j.renene.2014.06.019.